PERGAMON

International Journal of Heat and Mass Transfer 44 (2001) 1777–1787

International Journal of HEAT and MASS TRANSFER

www.elsevier.com/locate/ijhmt

TLCT and LDV measurements of heat transfer and fluid flow in a rotating sharp turning duct

T.-M. Liou [a,*], C.-C. Chen [b], M.-Y. Chen [a]

[a] *Department of Power Mechanical Engineering, National Tsing Hua University, Hsinchu 30043, Taiwan, ROC*
[b] *Microsystems Laboratory, Industrial Technology Research Institute, Hsinchu 30043, Taiwan, ROC*

Received 3 September 1999; received in revised form 19 May 2000

Abstract

Heat transfer measurements using a transient liquid crystal thermometry (TLCT) are presented to study the effect of rotation on the local heat transfer distributions around a sharp 180° turn of a two-pass smooth square duct for the first time in open literature. The duct has a dimensionless divider wall thickness of 0.25. Detailed local Nusselt number distributions on the leading and trailing walls are given for rotation numbers ranging from $Ro = 0$ to 0.20 at a Reynolds number of 1.0×10^4. The results show informative spanwise variations of heat transfer enhancement or abatement resulting from rotation. A critical range of Ro is identified, below which the regional averaged Nusselt number ratios of the regions after the 180° sharp turn in a rotating two-pass cooling passage are rather insensitive to the rotation effect. Laser–Doppler velocimetry (LDV) measurements within the turn are further performed to explain the local heat transfer distributions. Under rotating conditions, the curvature induced symmetric Dean vortices in the turn for the stationary case change greatly and are dominated by a single vortex most of which impinges directly on the leading wall's outer part, resulting in a high heat transfer enhancement on the leading wall in the turn.

1. Introduction

Internal cooling passages with 180° sharp turns are encountered in many applications. One of the examples is the internal cooling path of advanced gas turbine blades. Heat transfer around a 180° turn is affected by flow characteristics, such as the curvature-induced Dean-type vortices inside the turn, turn-induced separating bubble immediately downstream of the turn, and resulting high turbulence intensity levels [1], which are, in turn, influenced by rotation. The effects of rotation on heat transfer in a two-pass smooth square duct with a 180° straight-corner turn are therefore an important issue but the detailed information regarding heat transfer distributions under rotating conditions is still limited in open literature.

Most prior heat transfer studies relevant to 180° turning flows under rotation are based on thermocouple measurements. Wagner et al. [2,3] experimentally studied turbulent heat transfer in a four-pass serpentine square-sectioned channel with smooth walls. Large changes on heat transfer were found for radially outward flows due to variations of density ratio and rotation number while relative small changes were found for radially inward flow. Yang et al. [4] performed thermocouple measurements for turbulent flows in a four-pass serpentine square channel at low rotational speeds. Duct rotation was found to have a great effect on the value of local Nusselt number but little effect on circumferentially averaged values. Han et al. [5,6] experimentally studied uneven wall temperature effect on local heat transfer for turbulent flows in a rotating two-pass square channel with smooth wall. Although aforementioned heat transfer studies based on thermocouple measurements had provided valuable information, the reported heat transfer coefficients were discrete and regional averaged values.

* Corresponding author. Tel.: +886-3-5742607; fax: +886-3-5729716.
E-mail address: tmliou@pme.nthu.edu.tw (T.-M. Liou).

0017-9310/01/$ - see front matter
PII: S0017-9310(00)00221-0

Nomenclature

A half width of duct (m)
B half height of duct (m)
C_p specific heat (J kg^{-1} K^{-1})
D_H hydraulic diameter, $4AB/(A+B)$ (m)
h heat transfer coefficient (W m^{-2} K^{-1})
TKE turbulent kinetic energy $(\overline{u^2}+\overline{v^2})/2$ (m^2 s^{-2})
k_a thermal conductivity of air (W m^{-1} K^{-1})
k_w thermal conductivity of wall (W m^{-1}K^{-1})
Nu local Nusselt number, hD_H/k_a
Nu_0 Nusselt number in fully developed tube flow $= 0.023Re^{0.8}Pr^{0.4}$
$\overline{\mathrm{Nu}}$ total averaged Nusselt number, $\overline{h}D_H/k_a$
Pr Prandtl number of air, $\rho C_p v/k_a$
Re Reynolds number, $U_b D_H/v$
Ro rotation number, $\Omega D_H/U_b$
T_i initial temperature of wall (K)
T_r bulk mean temperature of main stream (K)
T_w wall temperature is the liquid crystal green-point temperature (K)
U streamwise mean velocity (m s^{-1})
U_b duct bulk mean velocity (m s^{-1})
u streamwise velocity fluctuation (m s^{-1})
V transverse mean velocity (m s^{-1})
v transverse velocity fluctuation (m s^{-1})
W spanwise mean velocity (m s^{-1})
W_1 width of first-pass duct (m)
W_2 width of second-pass duct (m)
W_d divider thickness (m)
W_d^* dimensionless divider thickness, $W_d/(W_1+W_2)$
w spanwise velocity fluctuation (m s^{-1})
X streamwise coordinate, Fig. 2
X^* normalized streamwise coordinate, X/D_H
Y transverse coordinate, Fig. 2
Y^* normalized transverse coordinate, Y/B
Z spanwise coordinate, Fig. 2
Z^*, Z^{**} normalized spanwise coordinate,
(i) $X<0$, $Z^{**}=Z/(2A+W_d)$ (in the turn)
(ii) $X\geqslant 0$, $Z<0$, $Z^*=(Z+W_d/2)/2A$ (in the first pass)
(iii) $X\geqslant 0$, $Z>0$, $Z^*=(Z-W_d/2)/2A$ (in the second pass)

Greek symbols
α_w thermal diffusivity of wall (m^2 s^{-1})
Ω rotating speed (rad s^{-1})
ρ air density (kg m^{-3})
v kinematic viscosity (m^2 s^{-1})
τ time step (s)

Subscripts
b bulk
rg regional average

The transient liquid crystal thermometry (TLCT) is generally superior to thermocouple technique in many aspects and has been used by some researchers. Ekkad and Han [7] used a transient liquid crystal image technique to measure local heat transfer distributions near a sharp 180° turn of a two-pass smooth square channel for Reynolds numbers of 1.0×10^4, 2.5×10^4, and 5.0×10^4. The heat transfer results were broadly consistent with the mass transfer results reported by Han et al. [8]. Liou et al. [9] recently performed heat transfer measurements by using a transient liquid crystal method. The effect of divider thickness on the local heat transfer distributions around a sharp 180° turn of a two-pass smooth square duct was examined. Ekkad and Han [10] reported Nusselt number distributions for a two-pass square channel with one ribbed wall based on the transient liquid crystal measurements. Chyu et al. [11] investigated heat transfer enhancement of ducts with multiple delta wing pair arrays by using a transient liquid crystal technique as well. In general, the transient liquid crystal technique is able to provide detailed local heat transfer distribution maps; nevertheless, its applications to study heat transfer associated with rotation channel are still unprecedented.

The present study aims at performing detailed measurements of the heat transfer coefficient in a straight-corner turn two-pass square duct with rotation using the transient liquid crystal method. Such an investigation has not been reported in the past. It is hoped that the data obtained herein lead to insight into the relevant physics and can be used for verifying ongoing computational predictions. Furthermore, as a continuation of Liou and Chen [1], complimentary laser-Doppler velocimetry (LDV) measurements of fluid flow in the rotating channel are used to explain the liquid crystal measured surface heat transfer distributions.

2. Method of approach

2.1. Test apparatus and conditions

Fig. 1 schematically depicts the thermochromatic liquid crystal imaging experimental setup and flow circuit. A digital video camera and a light source (white fluorescent lamps) fixed to the rotating test section were used to record the color change of the liquid crystal coating when the hot flow passed through the test sec-

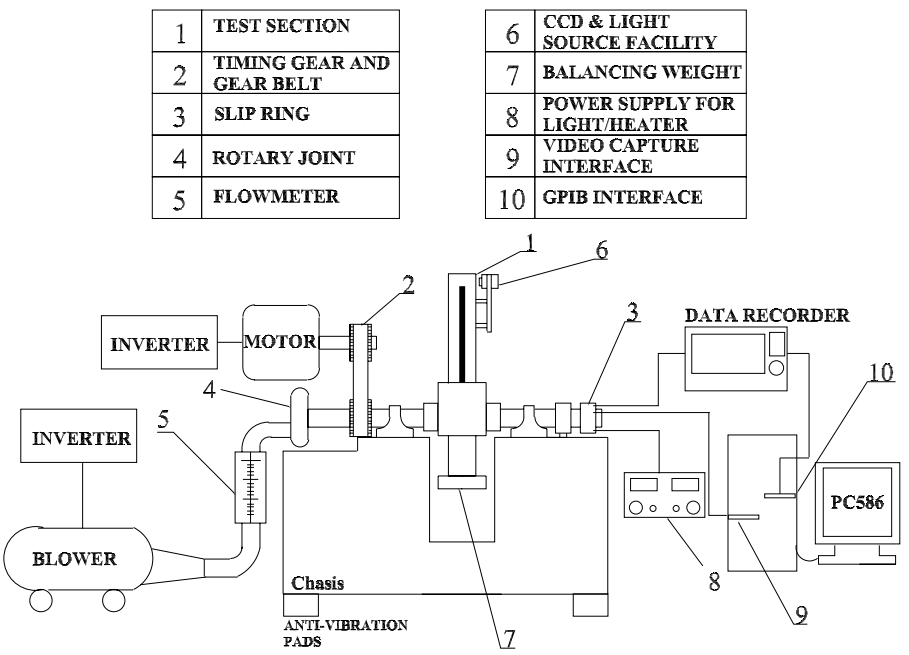

Fig. 1. The experimental setup of transient liquid crystal thermometry system.

tion. A two-channel thermocouple recorder measured the main flow temperatures at the upstream and downstream locations of the test section during the test. The junction-bead of the thermocouple was about 0.15 mm in diameter. All the data and power lines from the rotating part were connected to the stationary part via a 12-channel slip ring. The video and temperature data were then fed to a PC for post-processing. As shown in Fig. 2, the plenum cylinder was a part of the hollow shaft and was separated into two parts by the divider between the two passages. Ambient air was drafted into one side of the plenum cylinder in the hollow shaft, and then turned 90° sharply into the first radial passage in the rotor arm. Air passed by a rapid-response mesh heater (100 mm in length as shown in Fig. 2) and was heated. An additional length of 218 mm in front of the test section was functioned as the flow-developing region. The effect of entry turning may still remain for such a length; nevertheless, this is often encountered in a practical turbine blade's internal cooling passage. Air flowed radially outward in the first passage and radially inward in the second passage after making a 180° sharp turn. The "cooled" air from the test section flowed subsequently through the other side of the plenum cylinder in the hollow shaft, a rotary joint, a flexible pipe, a rotameter, and then was exhausted to ambient by a 2.2 kW turbo blower. A frequency inverter was used to adjust the blowing flow rate. Several rotameters ranging

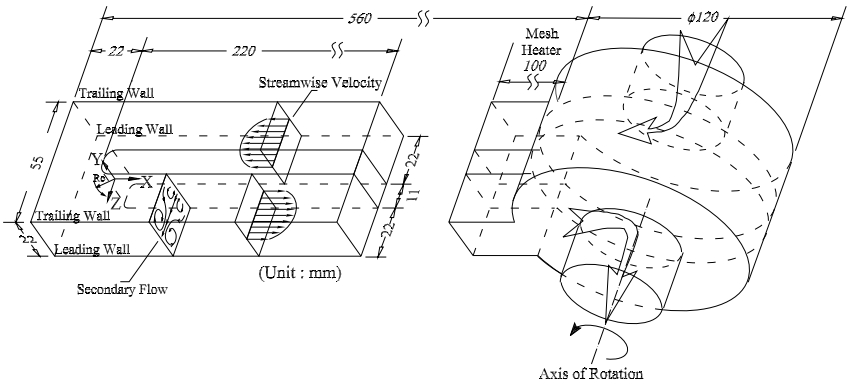

Fig. 2. Sketch of configuration, coordinate system, and dimensions of test section (flow patterns are for the case of $Ro = 0$).

from 100 to 2000 l/min were used to measure the coolant flow rate. The test section was made of thick acrylic sheets for optical access. The hydraulic diameter of the square cross-sectional flow path was $D_H = 22$ mm. At the turn, the clearance between the tip of the divider wall and the duct outer wall was fixed at $1D_H$ (or 22 mm). The divider-wall thicknesses examined was $W_d = 0.5D_H$ or $W_d^* = 0.25$ and Reynolds number, based on the bulk mean velocity and hydraulic diameter, was fixed at 1.0×10^4. The rotational speed range from 0 to 660 rpm corresponded to a rotation number range from 0 to 0.20. The heat transfer measurements were made in the region of $4.5D_H$ upstream to $4.5D_H$ downstream of the turn on the trailing and leading walls.

The LDV experimental setup for the complementary velocity measurements in the present work, as shown in Fig. 3, is basically the same as that described in the work of Liou and Chen [1]. Please refer to this earlier paper for more detail. The secondary-flow velocity vector mappings were performed at a mid-turn cross-section with $W_d^* = 0.06$. The Reynolds number was fixed at $Re = 1.4 \times 10^4$, and rotation number at $Ro = 0.10$. These conditions were selected to compare with the stationary part ($Re = 1.4 \times 10^4$ and $Ro = 0$) reported by Liou and Chen [1]. Quantitatively, the LDV measurements were also performed to reveal the rotation effect on the turbulence intensity distributions in the mid-turn cross-section.

2.2. Theory of liquid crystal thermometry

Given a semi-infinite wall that is initially at a uniform temperature ($T = T_i$ at $t = 0$), the surface of the wall is suddenly heated or cooled convectively with a fluid at a constant temperature or a bulk temperature T_b. A one-dimensional transient heat conduction analysis

$$\alpha \frac{\partial^2 T}{\partial Y^2} = \frac{\partial T}{\partial t} \tag{1}$$

over a semi-infinite solid medium with a convective boundary condition and assumptions of constant property and heat transfer coefficient values

$$-k\frac{\partial T}{\partial Y} = h(T_w - T_b) \quad \text{at } Y = 0,$$
$$T(Y,0) = T_i, \quad T(\infty,t) = T_i, \tag{2}$$

gives the dimensionless wall temperature T_w for the test surface as follows:

$$\frac{T_w - T_i}{T_b - T_i} = 1 - \exp\left(\frac{h^2\alpha_w t}{k_w^2}\right)\operatorname{erfc}\left(\frac{h\sqrt{\alpha_w t}}{k_w}\right). \tag{3}$$

When T_i, T_b, and the time, t, for T_w attaining the green point are given, the local heat transfer coefficient, h, over the test surface coated with liquid crystals can be calculated from Eq. (3). The green point is the temperature at which the liquid crystal appears green with the largest light intensity. The local bulk mean temperature $T_b(X)$ can be calculated by the interpolation of inlet and outlet coolant temperature. Due to the inability of performing an abrupt-change of the main air temperature during the transient test, the time history (Fig. 4) of the main stream air temperature is reproduced as a series of step functions. Using the Duhamel's superposition theorem, Eq. (3) can be rewritten as Eq. (4)

$$T_w - T_i = \sum_{j=1}^{N} \times \left[1 - \exp\left(\frac{h^2\alpha_w(t-\tau_j)}{k_w^2}\right)\operatorname{erfc}\left(\frac{h\sqrt{\alpha_w(t-\tau_j)}}{k_w}\right)\right][\Delta T_r], \tag{4}$$

where ΔT_r and τ_j are the temperature and time step changes from the recorder output. The local heat transfer coefficient at a given point on the measured region is thus actually obtained by solving Eq. (4).

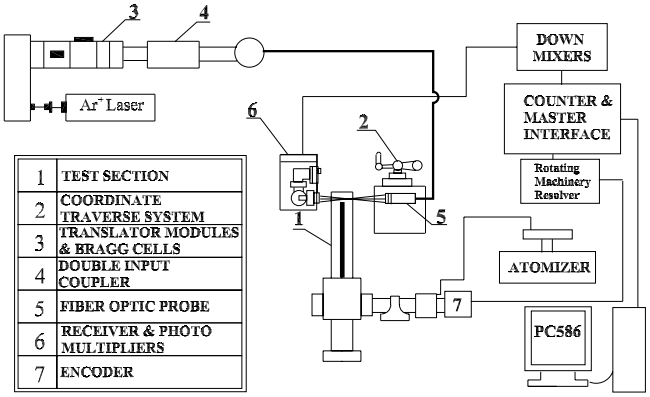

Fig. 3. The experimental setup of laser-Doppler velocimetry system.

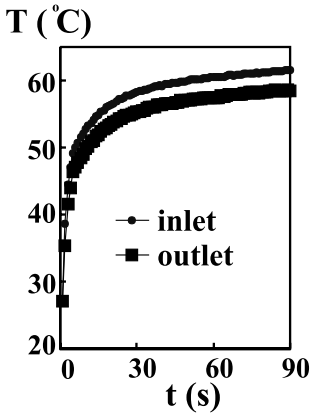

Fig. 4. Mainstream temperature variations during the transient test.

2.3. Uncertainty estimation

The non-dimensional uncertainty intervals for the variables in Eq. (3) are listed as follows:

Time of color change	t	±3.5%
Thermal diffusivity of wall	α_w	±5.0%
Thermal conductivity of wall	k_w	±5.0%
Bulk mean temperature of main stream	T_r	±5.5%
Green-point temperature	T_w	±1.5%
Initial temperature of wall	T_i	±1.5%

According to root-sum-square method, the most proper uncertainty is estimated to be ±10%. Conduction losses are relatively small because the transient test period is short and the walls are made of insulating material. Radiation is negligible because the entire walls of the channel are heated by the mainstream at fairly uniform temperature.

The statistical errors in the mean velocity and turbulence intensity were less than 1.8% and 3.1%, respectively, for a 95% confidence level. More detailed uncertainty estimates and velocity bias correlations are included in Liou and Chen [1]. For the range of atomizer pressure setting used, the saline solution was mixed to produce particles from 0.5 to 1.2 μm. This particle diameter range is able to follow turbulence frequencies exceeding 1 kHz [12].

3. Results and discussion

The local Nusselt number distributions on the $Y^* = -1$ wall ($Ro = 0$), trailing wall ($Y^* = 1$, for $0 < Ro \leqslant 0.20$), and leading wall ($Y^* = -1$, for $0 < Ro \leqslant 0.20$) are presented. The test surface is divided into 11 regions to evaluate regional averaged Nusselt number ratio. Furthermore, local spanwise Nusselt number ratio distributions are presented at six selected stages to document the rotating effect on the local heat transfer enhancement and decrement.

3.1. Local Nu distribution

Fig. 5 shows the detailed local Nusselt number ratio Nu/Nu_0 distributions on the wall ($Y^* = -1$) for $Ro = 0$. The local Nusselt number ratio is based on the Dittus–Boelter correlation for a stationary smooth circular tube ($Nu_0 = 0.023Re^{0.8}Pr^{0.4}$) [13]. In the first pass, the local Nusselt number ratios are dropped steadily from 1.2 at $X^* = 4$ to 1.0 at $X^* = 0$, suggesting that the flow is thermal fully developed at the end of the first pass. Generally, the 180° sharp turn has no prominent effect on the heat transfer in the first pass. As the flow enters the turn, higher local Nusselt number ratios are observed away from the divider wall. This is mainly due to the turn induced Dean-type secondary flow [1] which impinges directly onto the regions near the outer wall ($X^* = -1$). In the second pass, the heat transfer still prevailed near the outer wall ($Z^* = 1$) where Nusselt number ratio has the highest value ($Nu/Nu_0 \sim 4$) around X^* from −1 to 1. The lower heat transfer zone near the divider tip ($X^* = 0, Z^* = 0$) and the inner wall ($X^* = 0$–$1, Z^* = 0$) is generally due to the existence of a turn-induced separation bubble [1]. As can be seen from Fig. 5, the heat transfer rate drops as the flow redevelops, e.g., $Nu/Nu_0 \approx 2.2$ and $Nu/Nu_0 \approx 1.2$ at $X^* = 2.5$ and $X^* = 4.5$ of the second pass, respectively.

Figs. 6–9 show the detailed local Nusselt number ratio distributions on the leading and trailing walls for the rotating case. It is found that even a slight rotation with $Ro = 0.01$ affects the heat transfer distribution in the 180° sharp turn, as evidenced from Fig. 6. The most distinct variation occurs near the outer wall ($X^* = -1$) inside the turn, where Nu/Nu_0 increases and slightly decreases on the leading wall (Fig. 6(a)) and trailing wall (Fig. 6(b)), respectively. In the first pass, the Nu/Nu_0 on the trailing wall also increases slightly from those of the stationary case. Fig. 7 shows detailed local Nusselt

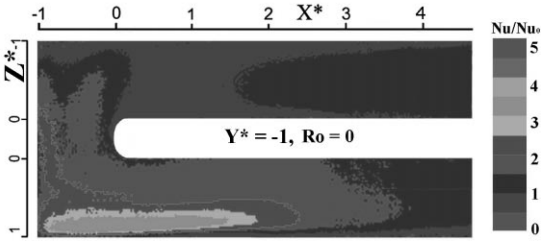

Fig. 5. Detailed local Nusselt number ratio Nu/Nu_0 distributions on the wall ($Y^* = -1$) for $Ro = 0$.

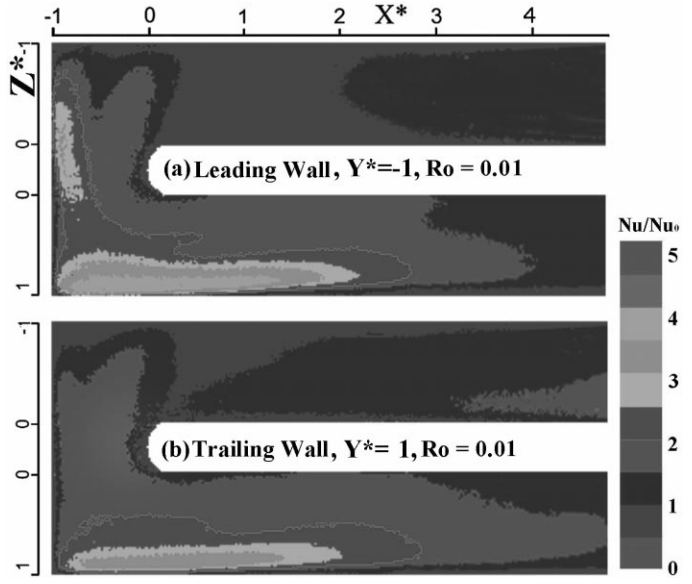

Fig. 6. Detailed local Nusselt number ratio Nu/Nu_0 distributions for $Ro = 0.01$ on (a) leading wall, and (b) trailing wall.

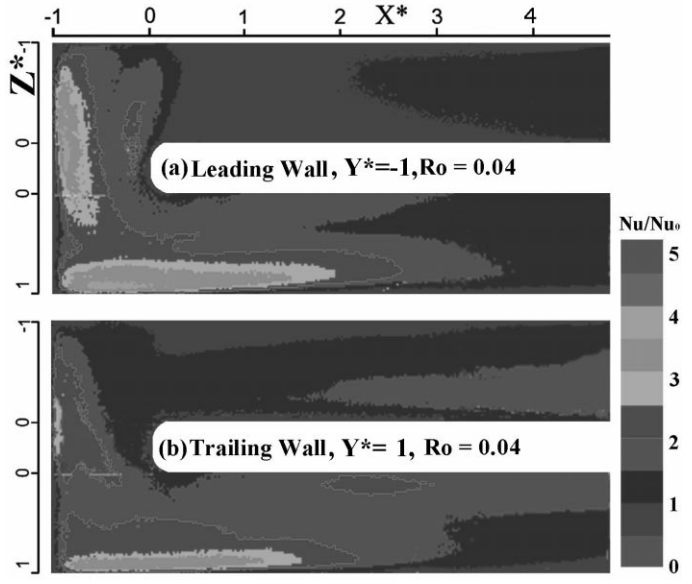

Fig. 7. Detailed local Nusselt number ratio Nu/Nu_0 distributions for $Ro = 0.04$ on (a) leading wall, and (b) trailing wall.

number ratio distributions for $Ro = 0.04$. The outer part of the leading wall inside the turn ($X^* < -0.5$ on Fig. 7(a)) is still the most heat-transfer-elevated area in comparison with the stationary case (Fig. 5). In the two passes, an obvious variation occurs on the trailing wall, where the relatively higher Nu/Nu_0 color band (the sky blue) skews toward the divider wall. Also note that a green spot appears around $X^* = 2.3$ and $Z^* = 0$ in the second pass.

For a moderate rotation number, e.g., $Ro = 0.10$, rotation results in a prominent heat transfer redistribution in the internal cooling channel, as evidenced from a comparison of Fig. 8 with Fig. 7 or Fig. 5. In the first pass, the Nu/Nu_0 on the leading wall decreases from those of the stationary case while Nu/Nu_0 increases on the trailing wall distinctly. In the second pass, rotation causes an overall rise of Nu/Nu_0. The leading wall has a superior heat transfer enhancement ($Nu/Nu_0 = 3$–5) in

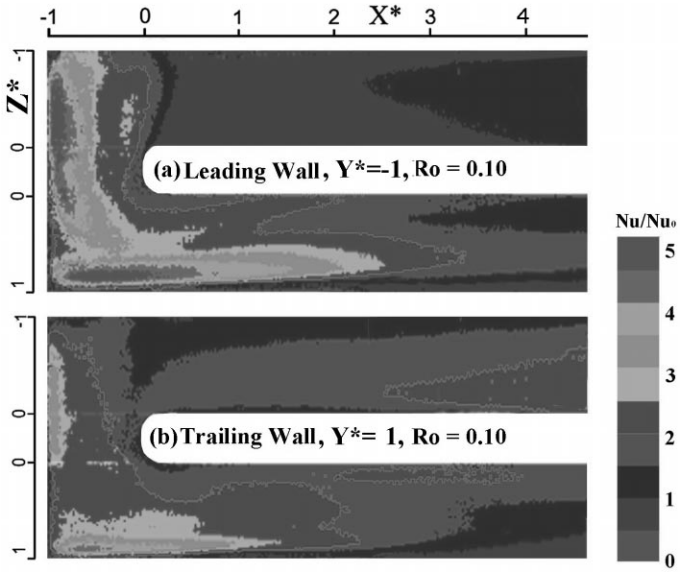

Fig. 8. Detailed local Nusselt number ratio Nu/Nu_0 distributions for $Ro = 0.10$ on (a) leading wall, and (b) trailing wall.

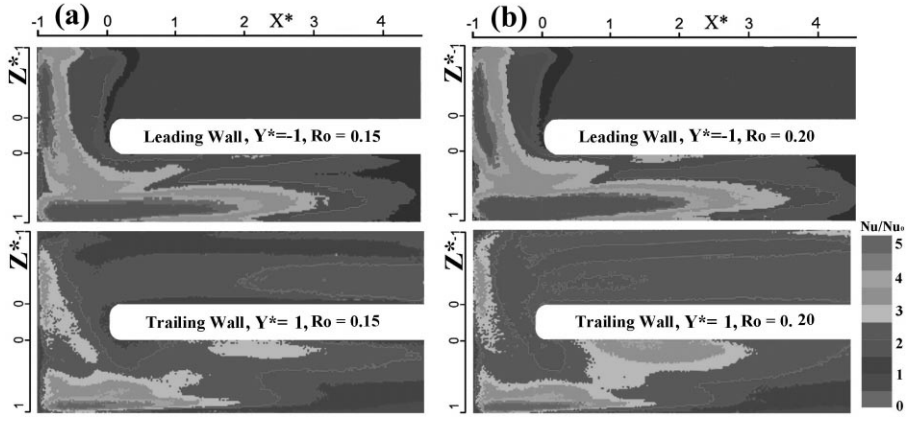

Fig. 9. Detailed local Nusselt number ratio Nu/Nu_0 distributions on the leading and trailing walls at high rotation numbers: (a) $Ro = 0.15$, and (b) $Ro = 0.20$.

the region from $X^* = 0$ to $X^* = 3$. The spanwise variations originating from rotation, not reported in open literature, are also presented in Figs. 8(a) and (b). The variations are most prominent in the second pass where duct rotation skews the higher heat transfer regions toward inner walls on the trailing walls. Leading wall within the turn is the best heat transfer augmentation region as a result of rotation. These phenomena resulting from the combining effects of duct rotation and turn will be illustrated by using the measured flow field results in the next section for a better comprehension. Making a comparison between the rotating and nonrotating cases, the highest local Nusselt number ratios are 3.8, 5.3, and 4.7 for the wall ($Y^* = -1$) at $Ro = 0$ (Fig. 5), the leading wall at $Ro = 0.10$ (Fig. 8(a)), and the trailing wall at $Ro = 0.10$ (Fig. 8(b)), respectively.

Fig. 9 displays the vivid development of the heat transfer distributions at even higher rotation numbers. It is found that on the trailing wall the heat transfer variation due to rotation is less obvious in the turn than in the two passes for rotation numbers ranging from $Ro = 0.15$ to 0.20. The phenomenon is opposite to those of lower Ro cases (Figs. 6–8), where the rotation-induced variations occur mainly inside the turn. A high heat transfer region is formed around $X^* = 2$ on the divider wall side in the second pass for both $Ro = 0.15$

and 0.20. In addition to the skewness of the higher heat transfer area toward the divider wall, higher Nu/Nu_0 is also found near the outer wall in the first pass. Therefore, a relative low heat transfer "gorge" is shaped in the first pass along $Z^* \approx -0.7$. All of these interesting revelations imply a much more complicated secondary flow for high rotation numbers, say, $Ro \geqslant 0.15$. The asymmetric heat transfer distribution in the first pass is caused by the entrance effect. In stationary conditions, the heat transfer distribution is quite symmetrical (as shown in Fig. 5) with respect to the pass centerline since the 90° turning effect is fading out through a developing length of about $15D_H$ (as shown in Fig. 2). Under rotation, however, the combined turning and rotating effects result in asymmetrical flow field as well as heat transfer. The degree of asymmetry in heat transfer increases with increasing Ro, analogical to the heat transfer results in the second pass. In other words, rotation has changed the entrance condition of the measuring area in the first pass.

3.2. Regional averaged Nu distribution

From Figs. 5–9, the regional averaged Nusselt number is calculated according to the region index layout shown in Fig. 10, and the results are also presented in Fig. 10. It is observed that the regional averaged Nusselt number ratio Nu_{rg}/Nu_0 distributions on the leading wall with rotation ($Ro = 0.01$–0.10) are 5–15% lower than those without rotation ($Ro = 0$) in the first pass (region indices: −5, −4, −3, and −2 in Fig. 10(a)). The Nu_{rg}/Nu_0 on the leading wall in the first pass decreases with increasing rotation number on a relatively small scale. On the leading wall, the Nu_{rg}/Nu_0 is mostly elevated in the turn (region indices: −1, 0, and 1). The regional averaged Nusselt number ratios are 12–17%, 18–55%, and 40–100% for $Ro = 0.01$, 0.04, and 0.10, respectively, higher than those without rotation ($Ro = 0$). Note that, on the leading wall, the entrance part of 180° sharp turn (region index: −1) has the highest rotation-induced heat transfer enhancement (two times of its stationary counter part for $Ro = 0.10$) among the examined regions and conditions. Immediately after the turn (region indices: 2 and 3), the Nu_{rg}/Nu_0 on the leading wall are 2–5%, 5–11%, and 12–25% for $Ro = 0.01$, 0.04, and 0.10, respectively, higher than those without rotation ($Ro = 0$). Generally, the rotation-induced heat transfer enhancement diminishes while the fluid flow proceeds away from the turn for Ro ranging from 0.01 to 0.10, as indicated in Fig. 10(a) that the data band narrows down from region index 1–3. For region index $\geqslant 4$, the differences in Nu_{rg}/Nu_0 on the leading wall between the rotatory and stationary cases drop to 2–8%.

In contrast to that occurring on the leading wall, rotation affects the heat transfer on the trailing wall in a quite different way. In the first pass (region indices:

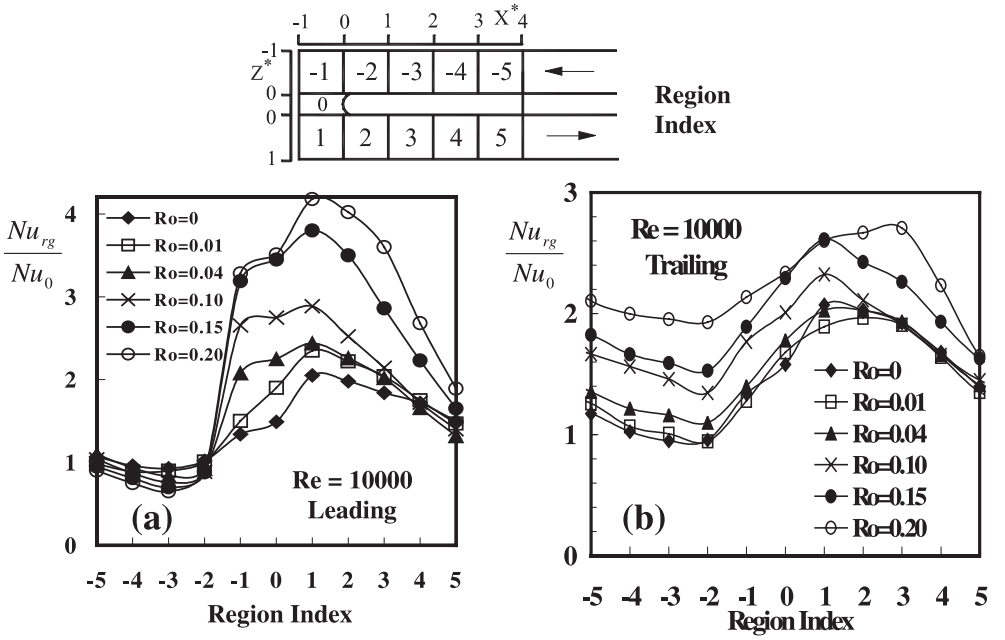

Fig. 10. Regional averaged Nusselt number ratio Nu_{rg}/Nu_0 distributions for various rotation numbers on (a) leading wall and (b) trailing wall.

−5, −4, −3, and −2 in Fig. 10(b)), the Nu_{rg}/Nu_0 on the trailing wall increases concurrently with increasing rotation number. The regional averaged Nusselt number ratios are 4–12%, 15–25%, 42–54%, 56–68%, and 80–106%, for $Ro = 0.01$, 0.04, 0.10, 0.15, and 0.20, respectively, higher than those without rotation ($Ro = 0$). Note that the highest heat transfer enhancement (2.1 times of its stationary counter part for $Ro = 0.20$) occurs at region index −2 on the trailing wall among the regions and conditions examined. Inside the turn, rotation-induced alteration on Nu_{rg}/Nu_0 distribution is quite similar to that occurring in the first pass, except for the cases with relatively high rotation numbers ($Ro \geqslant 0.15$). Figs. 9 and 10(b) indicate that the rotation-induced heat transfer enhancement ceases to increase as Ro is increased from 0.15 to 0.20 at the mid-turn (region index 0) and post-turn (region index 1) regions. After the turn (region index: 2–5), a critical range of rotation number, $0.10 < Ro_c \leqslant 0.15$, can be defined. That is, there exists a critical range of Ro_c below which rotation has no prominent effect on the regional averaged Nusselt number ratios ($Ro = 0.01$, 0.04, and 0.10 in Fig. 10(b)) on the trailing wall of the second pass. When rotation number is above Ro_c, the influence of rotation is presented definitely by the 15–28% and 19–41% enhancement of Nu_{rg}/Nu_0 for $Ro = 0.15$ and 0.20, respectively, as shown in Fig. 10(b). The above observation suggests that when Ro is larger than the Ro_c, the rotation effect on the heat transfer augmentation in the second pass will overtake the role previously dominated by the turning effect in the stationary or low rotation number cases.

3.3. Rotation effects on the secondary flow in the 180° turn

Fig. 11 shows the secondary-flow pattern at the mid-turn ($Z^{**} = 0$) cross-section for $W_d^* = 0.06$ under stationary and rotatory conditions. It is well known that a Dean-type secondary flow typically exists for a flow through a turn due to the imbalance of centrifugal force and pressure gradient, as shown by Fig. 11(a) [1]. In the stationary case, the counter-rotating Dean vortex pair appears symmetrically with the vortex centers locating at $X^* = -0.80$ and $Y^* = \pm 0.75$. The maximum cross-stream mean velocity occurs at $Y^* = 0$ near the divider tip ($X^* = -0.08$). Relatively low secondary-flow velocities appear around X^* from −0.4 to −0.7 near the walls ($Y^* = \pm 1$). Two regions with secondary flow directed toward the leading and trailing walls occur around $X^* = -1$ and Y^* from ±0.5 to ±1 where heat transfer is elevated. In particular, the downwash regions of the secondary flow are associated with the highest Nu/Nu_0 enhancement, as evidenced from Fig. 5.

As the duct rotates, Fig. 11(b) clearly reveals that the difference in Ro does affect the cross-stream flow pattern inside the turn. In the first pass of the rotating duct, the streamwise mean velocity profiles are skewed towards the trailing wall [1], as evidenced in Fig. 11(b) that most flow directs along the trailing wall around X^* from 0 to −0.5. Therefore, the symmetry of the turn-induced secondary flow is significantly altered, and the lower part of Dean vortex pair dominates the whole cross-section of mid-turn. The ruling vortex occupies 90% area of the mid-turn cross-section, and directs the major flow to impinge and sweep the leading wall. This is the main

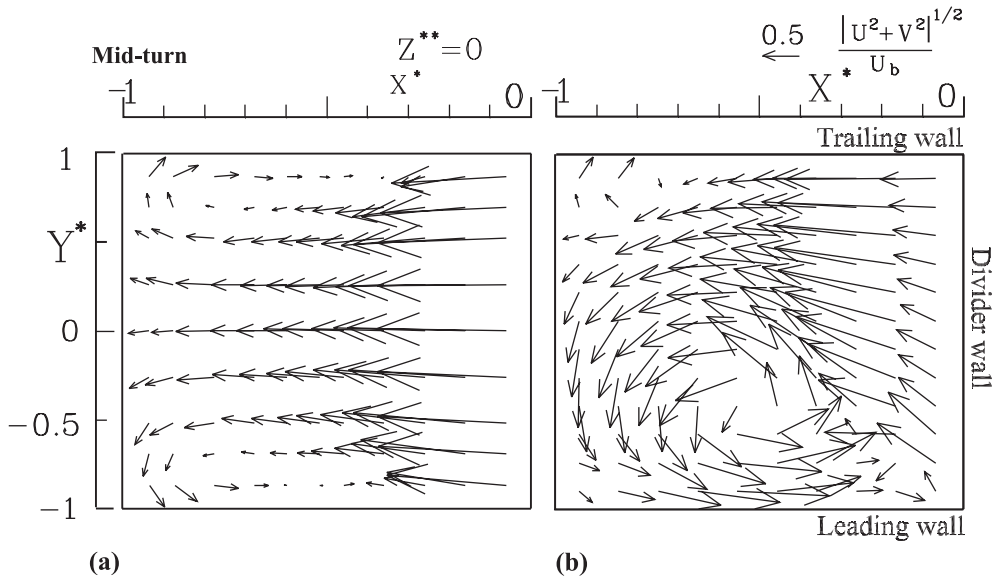

Fig. 11. Secondary flow patterns at mid-turn cross-section for $Re = 1.4 \times 10^4$: (a) $Ro = 0$ [1], and (b) $Ro = 0.10$.

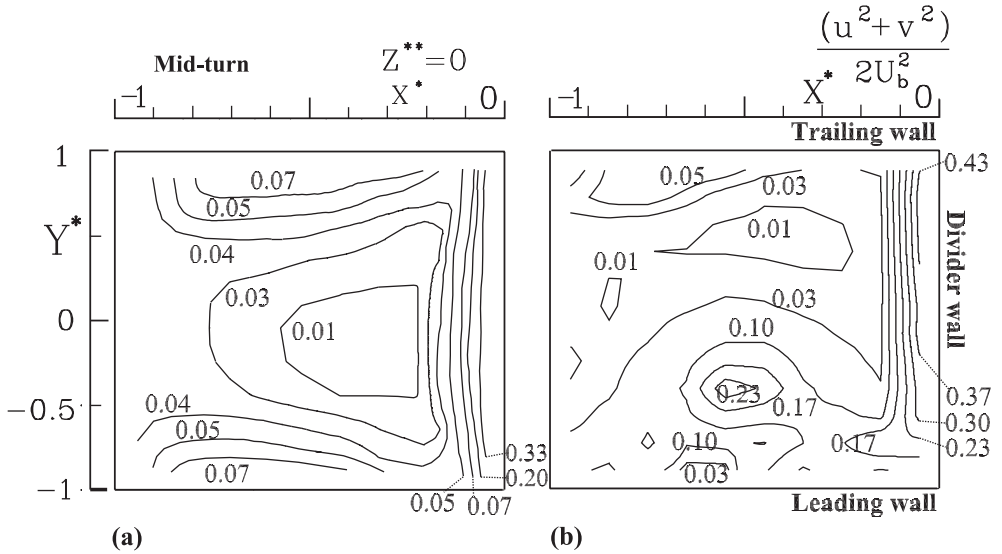

Fig. 12. Turbulent kinetic energy contours at mid-turn cross-section for $Re = 1.4 \times 10^4$: (a) $Ro = 0$, and (b) $Ro = 0.10$.

reason that the heat transfer enhancement is much greater on the leading wall than on the trailing wall in the 180° sharp turn (Fig. 8, $Ro = 0.10$). The upper part of the distorted Dean vortex pair still exists but is confined to the upper left corner ($Y^* > 0.7$ and $X^* < -0.8$). Although its size is small, the upper vortex has a larger normal component to the trailing wall than its stationary counter part, and thus contributes to the heat transfer enhancement on the mid-turn trailing wall, as shown in Figs. 7(b) and 8(b). A corner vortex is also found near the lower right corner ($X^* = 0$ and $Y^* = -1$) of the mid-turn cross-section. This rotation-induced vortex is formed by the collision of the two opposite streams – one is the main stream from the first pass and the other is the reverse flow of the dominative vortex in the turn – near the entrance of the turn ($X^* \sim 0$). Quantitatively, rotation increases the total averaged strength of secondary flow, $\overline{\sqrt{U^2 + V^2}}$, from $0.68U_b$ ($Ro = 0$) to $0.78U_b$ ($Ro = 0.10$) in the mid-turn cross-section. In particular, $\overline{\sqrt{U^2 + V^2}}$ is noticeably increased by rotation from $0.32U_b$ ($Ro = 0$) to $0.71U_b$ ($Ro = 0.10$) around the most-heat-transfer-elevated area ($Y^* < -0.7$ and $X^* < -0.2$ on the leading wall, Figs. 8(a) and 11).

In view of the large distortion of the secondary-flow mean velocity profiles by rotation in the mid-turn of the 180° sharp turn, the difference of turbulence distributions between rotating and non-rotating cases is expected to be obvious. Fig. 12 thus depicts the dimensionless turbulent kinetic energy (TKE) distribution in the corresponding region. Note that the TKE discussed here is composed of X and Y components. It is seen that the symmetric distribution of TKE for $Ro = 0$ is demolished by increasing Ro to 0.10. The highest local TKE peak near the divider wall is associated with the separation-bubble's shear layer [1] and is elevated from 0.33 ($Ro = 0$) to 0.43 ($Ro = 0.10$) by rotation. In the stationary case ($Ro = 0$), two higher TKE (0.07) regions are associated with the Dean-type vortex pair while a low TKE (0.01) region with the central main stream. In the rotating case ($Ro = 0.10$), the second highest peak of TKE (0.23) is generated around the center of the dominative vortex. In addition, the aforementioned rotation-induced single vortex derives one more high turbulence region (TKE = 0.17, X^* from 0 to −0.3 and Y^* from −0.6 to −1.0). As far as heat transfer enhancement in the mid-turn region is concerned, it is worthwhile of pointing out that the controlling fluid dynamics factor is more assumed by the direction and magnitude of the secondary-flow mean velocities than by the TKE as supported by the above discussion.

4. Conclusions

The following main results are drawn from the data presented:

1. The TLCT has been successfully implemented on the investigation of heat transfer enhancement in the rotating internal cooling channel for the first time. Duct rotation is found to have significant effects on the spanwise (Z-direction) heat transfer distribution. A result is difficult to being resolved by the regionally averaged analysis from the conventional thermocouple measurements.

2. The variations are most prominent in the second pass where duct rotation skews the higher heat transfer regions toward inner walls on the trailing walls.
3. There exists a critical range of rotation number, $0.10 < Ro_c \leqslant 0.15$. Below Ro_c, rotation has no prominent effect on the regional averaged Nusselt number ratios of the regions after the 180° sharp turn in a rotating two-pass cooling passage. This piece of information provides a useful reference of practical tests of computational models.
4. Duct rotation provides an overall enhancement on the heat transfer enhancement, except the slight abatement on the leading wall of the first pass.
5. The curvature induced symmetric Dean-type vortices in the mid-turn for the stationary case changes greatly with rotation. For the case of rotation, the cross-stream secondary flow in the mid-turn is gradually dominated by a single vortex most of which impinges directly on the outer part of leading wall, and thus greatly enhances heat transfer rate in the vicinity.
6. Duct rotation elevates noticeably the magnitude of the TKE of the secondary flow in the 180° sharp turn. Meanwhile, the symmetrical TKE contour for the stationary case is skewed and redistributed by rotation.

Acknowledgements

This paper was prepared with the support of the National Science Council of the Republic of China under contract NSC 88-TPC-E-007-017.

References

[1] T.M. Liou, C.C. Chen, LDV study of developing flows through a smooth duct with 180° straight-corner turn, ASME Journal of Turbomachinery 121 (1999) 167–174.
[2] J.H. Wagner, B.V. Johnson, T.J. Hajek, Heat transfer in rotating passages with smooth walls and radial outward flow, ASME Journal of Turbomachinery 113 (1991) 42–51.
[3] J.H. Wagner, B.V. Johnson, F.C. Kopper, Heat transfer in rotating serpentine passages with smooth walls, ASME Journal of Turbomachinery 113 (1991) 321–330.
[4] W.J. Yang, N. Zhang, J. Chiou, Local heat transfer in a rotating serpentine flow passage, ASME Journal of Heat Transfer 114 (1992) 354–361.
[5] J.C. Han, Y.M. Zhang, Effect of uneven wall temperature on local heat transfer in a rotating square channel with smooth walls and radial outward flow, ASME Journal of Heat Transfer 114 (1992) 850–858.
[6] J.C. Han, Y.M. Zhang, K. Kalkuehler, Uneven wall temperature effect on local heat transfer in a rotating two-pass square channel smooth walls, ASME Journal of Heat Transfer 115 (1993) 912–920.
[7] S.V. Ekkad, J.C. Han, Local heat transfer distributions near a sharp 180° turn of a two-pass smooth square channel using a transient liquid crystal image technique, Journal of Flow Visualization and Image Processing 2 (1995) 285–297.
[8] J.C. Han, P.R. Chandra, S.C. Lau, Local heat/mass transfer distributions around sharp 180° turns in two-pass smooth and rib-roughened channels, ASME Journal of Heat Transfer 110 (1988) 91–98.
[9] T.M. Liou, C.C. Chen, T.W. Tsai, Liquid crystal measurements of heat transfer in a 180° sharp turning duct with different divider thicknesses, in: Proceedings of the 8th International Symposium on Flow Visualisation, Sorrento, Italy, 1998.
[10] S.V. Ekkad, J.C. Han, Local heat transfer distributions near a sharp 180° turn of a two-pass smooth square channel using a transient liquid crystal image technique, Journal of Flow Visualization and Image Processing 2 (1995) 285–297.
[11] M.K. Chyu, H. Ding, J.P. Downs, A. Van Sutendael, F.O. Soechting, Determination of local heat transfer coefficient based on bulk mean temperature using a transient liquid crystal technique, ASME Paper, No. 97-GT-489, 1997.
[12] F. Durst, A. Melling, J.H. Whitelaw, Principles and Practice of Laser-Doppler Anemometry, Academic Press, New York, 1976 (Chapter 9).
[13] F.W. Dittus, L.M.K. Boelter, Publications in Engineering, vol. 2, University of California of Berkley, Berkley, CA, 1930, p. 443.